

Spinal Canal and Spinal Marrow Segmentation by Means of the Hough Transform of Special Classes of Curves

Annalisa Perasso¹(✉), Cristina Campi¹,
Anna Maria Massone¹, and Mauro C. Beltrametti²

¹ CNR-SPIN, Genova, Italy

{perasso,campi}@dima.unige.it, annamaria.massone@cnr.it

² Dipartimento di Matematica, Università degli Studi di Genova, Genova, Italy
beltrametti@dima.unige.it

Abstract. In this paper we present a Hough Transform-based method for the detection of the spinal district in X-ray Computed Tomography (CT) images in order to build binary masks that can be applied to functional images to infer information on the metabolic activity of the spinal marrow. This kind of information may be of particular interest for the study of the spinal marrow physiology in both health and disease.

Keywords: Hough transform · Tomographic imaging · Image segmentation · Algebraic plane curves

1 Introduction

Hough Transform (HT) [1] is a classical pattern recognition technique commonly used to recognize profiles of interest in images. Its early formulation provided a strategy to detect just straight lines but it has been first extended to ellipse and circle recognition [2], and then generalized to arbitrary shape detection by means of look-up tables [3]. Recently, an extension to special classes of algebraic plane curves has been proposed in [4], and applications of this method to real astronomical and medical data have been presented in [5]. Here we want to apply this method to the case of the human spinal marrow and spinal canal segmentation in X-ray Computed Tomography (CT) images, bearing in mind clinical applications concerned with neurological diseases. In fact, it is very interesting to study how such disorders affect the spinal marrow, i.e., the elongated central nervous system tissue, which is contained in the spinal canal. The combination of different medical imaging techniques like X-ray CT and Positron Emission Tomography (PET) provides encouraging results for the study of neurological diseases [6]. The anatomical information coming from high resolution CT images are indeed very useful to exactly identify on the low resolution PET images the regions from which to extract the metabolic information. Unlike the case of Magnetic Resonance Imaging [7,8], in CT images the main problem which is

encountered in discriminating the spinal marrow within the spinal canal is due to the low contrast between the spinal marrow and the surrounding tissue. In [9], exploiting high local contrast between bone and spinal canal, an automated region growing algorithm is used for the spinal canal detection, while spinal cord detection is performed on the basis of geometrical arguments as the maximal inscribed circle in the polygon representing the spinal canal. In this paper we use the classical HT for ellipse detection, and its extension to special classes of algebraic plane curves, for an automated recognition of both the spinal marrow and the spinal canal in CT images, in order to build digital masks that can be applied to PET images.

The paper is organized as follows. In Section 2 we recall some basic concepts concerning the HT for algebraic plane curves, we present the family of curves we are interested in, and we study in detail the properties of the corresponding HT. Then in Section 3 we show the application to real CT images in order to identify both, the spinal marrow and the spinal canal, and we show the consequent integration with PET functional information. Finally, we offer our conclusions and comments in Section 4.

2 Background Material and Methods

We follow the notation introduced in [4,5]. Let us consider a family of irreducible polynomials in the variables X, Y ,

$$F(X, Y; \lambda) = \sum_{i,j=0}^d g_{ij}(\lambda) X^i Y^j, \quad 0 \leq i + j \leq d, \tag{1}$$

where the coefficients $g_{ij}(\lambda)$ are real polynomials in the independent parameters $\lambda = (\lambda_1, \dots, \lambda_t)$ varying in an Euclidean open set $\mathcal{U} \subseteq \mathbb{R}^t$, and with the degree, d , of $F(X, Y; \lambda)$ not depending on λ . Let \mathcal{F} be the corresponding family of zero loci \mathcal{C}_λ of $F(X, Y; \lambda)$, and assume that each \mathcal{C}_λ is a real curve in the affine plane $\mathbb{A}_{(X,Y)}^2(\mathbb{R})$. So we want a family $\mathcal{F} = \{\mathcal{C}_\lambda\}$ of irreducible curves which share the degree.

If $P = (x_P, y_P)$ is a point of $\mathbb{A}_{(X,Y)}^2(\mathbb{R})$, then the *Hough Transform* of P (with respect to the family \mathcal{F}) is the locus of the affine space $\mathbb{A}_{(A_1, \dots, A_t)}^t(\mathbb{R})$ of equation $\Gamma_P(A) : F(x_P, y_P; A) = 0$, where

$$\Gamma_P(A) = \sum_{i,j=0}^d g_{ij}(A) x_P^i y_P^j, \quad 0 \leq i + j \leq d,$$

is a real polynomial in the indeterminates $A = (A_1, \dots, A_t)$. For a general point P , $\Gamma_P(A)$ is a hypersurface. Thanks to [4, Lemma 2.3], we can say that the condition

$$\mathcal{C}_\lambda = \mathcal{C}_{\lambda'} \implies \lambda = \lambda' \quad \forall \mathcal{C}_\lambda, \mathcal{C}_{\lambda'} \in \mathcal{F} \tag{2}$$

is equivalent to

$$\bigcap_{P \in \mathcal{C}_\lambda} \Gamma_P(A) = \{\lambda\}. \tag{3}$$

Condition (3) is easy to be translated into a discrete framework for curve recognition in images: provided that an edge detection process selects in the image a set of points of interest potentially lying on the curve to be recognized, the intersection of their HTs leads to the identification of the parameter set characterizing the curve. Thus, we look for families of curves which satisfy the above equivalent conditions. Such families are called *Hough regular*. Condition (2) provides an effective way to check condition (3). In fact, the equality $\mathcal{C}_\lambda = \mathcal{C}_{\lambda'}$ is equivalent to $F(X, Y; \lambda) = kF(X, Y; \lambda')$ for some non-zero constant k . This leads to solve a polynomial system, in the variables $\lambda = (\lambda_1, \dots, \lambda_t)$, $\lambda' = (\lambda'_1, \dots, \lambda'_t)$, made up of the equations $g_{ij}(\lambda) = kg_{ij}(\lambda')$ for each pair of indices i, j . Therefore, saying that a family is Hough regular simply means that such a polynomial system implies $\lambda = \lambda'$. The two families of curves we will use in the sequel meet the above Hough regularity condition (see also [5, Section 3]).

Based upon the above theoretical result, then a recognition algorithm can be implemented as described in [5, Section 4], to which we refer for more details. Here, we confine ourselves to highlight the main steps of the process. First of all, we apply to the image an edge detection technique to select P_1, \dots, P_ν points of interest. Then, we discretize the parameter space by means of an appropriate number of cells and for each point P_i , $i = 1, \dots, \nu$, we compute the Hough Transform $I_{P_i}(A)$ with respect to a fixed family of curves. Next, we apply an accumulator function to count how many times each cell in the parameter space is crossed (voted) by the computed HTs. Finally, we look for the cell corresponding to the maximum of the accumulator function: the parameter set associated to that cell provides the curve of the family which best approximates the profile of interest in the image.

Remark 1. The application of an edge detection algorithm to select the points that will be processed with the HT technique has two advantages. First, grey levels of the image pixels can be forgotten; second, the number of points to process is dramatically reduced.

Remark 2. The computation of the accumulator function and its maximization is the most time-consuming step of the algorithm. Further, it strongly depends on the number of parameters, since the dimension of the domain of this function exactly corresponds to the number of parameters in the game. Even though the theory, and the algorithmic aspects, presented in this section hold true in the above general framework, in practice, the computational burden associated to the accumulator function computation and optimization leads to the need of restricting to families of curves depending on a small number of parameters. Work to overcome such a restriction is in progress.

2.1 Curve with 3 Convexities

As highlighted by the results of [5] (see in particular subsection 5.1 and Figure 6) the family of curves with 3 convexities, expressed by the equation in form (5) below, looks as a suitable family of curves to optimally detect the spinal canal

profile. In addition, to recognize the spinal marrow profile, ellipses in the form presented in Section 3 seem good candidate curves.

Generally speaking, we are well-aware of the fact that our approach strongly depends on the choice of a suitable family \mathcal{F} of curves to optimally recognize a given profile. Work to perform an automated search of an appropriate family \mathcal{F} is strictly related to the question raised in Remark 2 above. Even though in progress, it is not accomplished at the present state-of-the-art. On the other hand, let us stress how a good choice of the family \mathcal{F} makes the HT-based procedure extremely robust even in presence of noise (see also [4, Section 6]).

The *curve with m convexities* is defined by the polar equation

$$\mathcal{C}_{a,b,m} : \rho = \frac{a}{1 + b \cos(m\theta)}, \tag{4}$$

where a, b are real positive numbers such that $b < 1$, and $m \geq 2$ is an integer.

The curve with m convexities is bounded. In fact, computing the derivative with respect to θ in equation (4) we find

$$\rho' = \frac{abm \sin(m\theta)}{(1 + b \cos(m\theta))^2}.$$

Therefore $\rho' = 0$ if and only if $\theta = \frac{k}{m}\pi$ for some integer k . For such values of θ , equation (4) gives

$$\rho_{\min} := \frac{a}{1 + b}, \quad \rho_{\max} := \frac{a}{1 - b}$$

according to whether k is even or odd, respectively. Thus, the graph of the curve is contained in the circular crown of radii $\frac{a}{1+b}, \frac{a}{1-b}$. The special case $m = 3$ looks of interest for us. In this case, the curve has degree 6 and a direct computation yields the cartesian equation

$$\mathcal{C}_{a,b} : (X^2 + Y^2)^3 = (a(X^2 + Y^2) - b(X^3 - 3XY^2))^2. \tag{5}$$

The shape of the curve with 3 convexities strongly depends on the values of the parameters. In particular, a is a sort of scale factor, while, as much as the value of b increases as much the convexities of the curve are sharpened. Figure 1 shows the curve for three different values of b with a fixed to 1.

As far as the HT is concerned, fix a point $P = (x_P, y_P)$ in the image space $\mathbb{A}^2_{(X,Y)}(\mathbb{R})$. Then the HT of P with respect to the family $\mathcal{F} = \{\mathcal{C}_{a,b}\}$ is a degenerate conic $\Gamma_P(A, B) : r_- \cup r_+$ in the parameter plane $\mathbb{A}^2_{(A,B)}(\mathbb{R})$, i.e., the union of the parallel lines

$$r_{\mp} : A(x_P^2 + y_P^2) - B(x_P^3 - 3x_P y_P^2) \mp \sqrt{(x_P^2 + y_P^2)^3} = 0.$$

The fact that $\Gamma_P(A, B)$ is a degenerate conic could make the maximization of the accumulator function particularly challenging. It is then worth noting that the line

$$r_+ : A(x_P^2 + y_P^2) - B(x_P^3 - 3x_P y_P^2) + \sqrt{(x_P^2 + y_P^2)^3} = 0$$

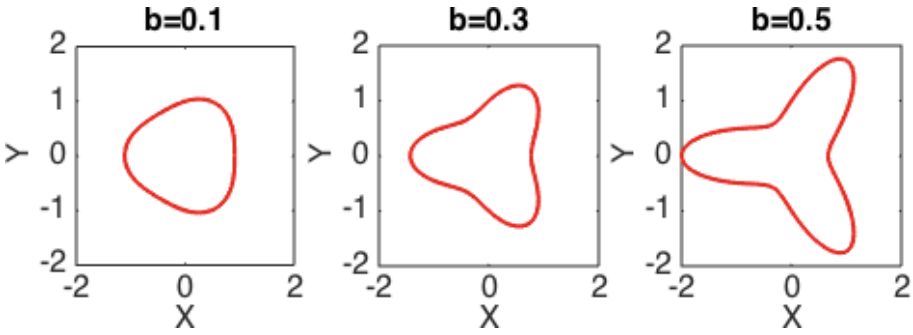


Fig. 1. Three curves with 3 convexities with $a = 1$ and, from left to right, $b = 0.1$, $b = 0.3$, and $b = 0.5$.

results in fact out of the game in our context. That is, in practice, the HT of P can be assumed to be the single line of equation

$$r_- : A(x_P^2 + y_P^2) - B(x_P^3 - 3x_P y_P^2) - \sqrt{(x_P^2 + y_P^2)^3} = 0.$$

First, note that the line r_+ intersects the negative A -axis of the parameter space $\mathbb{A}_{(A,B)}^2(\mathbb{R})$ in the point $\left(-\frac{\sqrt{(x_P^2 + y_P^2)^3}}{x_P^2 + y_P^2}, 0\right)$. Let

$$b_+ := \frac{\sqrt{(x_P^2 + y_P^2)^3}}{x_P^3 - 3x_P y_P^2}$$

be the ordinate of the point where the line r_+ intersects the B -axis. As the region of interest, \mathcal{T} , to be discretized is defined by the conditions $a > 0, 1 > b > 0$, it is then enough to show the inequality

$$b_+ \geq 1, \tag{6}$$

which implies that the line r_+ doesn't cross the region \mathcal{T} . This follows as soon as we show that

$$(X^2 + Y^2)^3 - (3XY^2 - X^3)^2 \geq 0, \tag{7}$$

or

$$Y^6 + 9X^4Y^2 - 6X^2Y^4 = Y^2(Y^4 + 9X^4 - 6X^2Y^2) = Y^2(Y^2 - 3X^2)^2 \geq 0,$$

which is, in fact, the case. Let's also point out that all the above agrees with the fact the family \mathcal{F} is Hough regular.

3 Applications

In order to study the metabolic activity of the spinal district in a human being, we have considered a stack of CT images of a control subject corresponding to

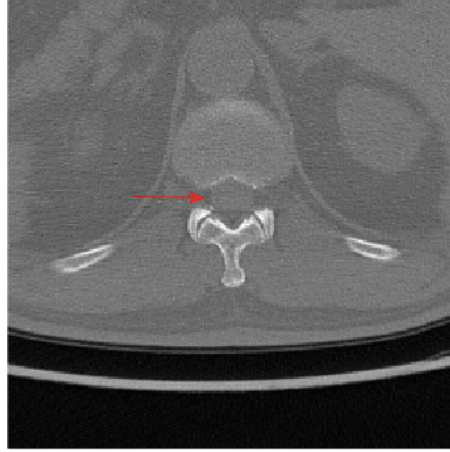


Fig. 2. Zoom of a CT image with focus on the spinal canal. It is possible to see the structure of both the spinal canal and the spinal marrow, the highlighted circular region inside the spinal canal.

a whole body acquisition. Note that the spinal marrow is situated in the upper part of the vertebral column, between the occipital bone and the first and the second lumbar vertebra. For this reason, we have limited our analysis just to the cervical and thoracic segments, for a total of 90 axial slices. In Figure 2 we show a detail of a CT image referring to a vertebra of this region, where it is possible to see the structure of both the spinal canal and the spinal marrow, i.e., the circular region inside the spinal canal, highlighted by the arrow.

For each slice, we first apply an edge detection algorithm [10] to get a set of points of interest (panel (a) in Figure 3). Then we compute the HTs of these points with respect to the family $\mathcal{F} = \{\mathcal{C}_{a,b}\}$ of curves with 3 convexities, and we take the parameters corresponding to the maximum of the accumulator function as those which identify the curve with 3 convexities best approximating the spinal canal profile in the image. The graph of such a curve (panel (b) in Figure 3) is then used to identify the region of the spinal canal. This step allows us to exclude the points outside of the canal. The points inside the graph of the curve (panel (c) in Figure 3) are the candidate points of interest for the recognition of the spinal marrow. We point out that, due to the very low local contrast between the spinal marrow and the surrounding tissue, it is hard for any edge detection algorithm to sample the whole profile of the spinal marrow. On the other hand, the HT procedure is very robust and effective in recognizing an entire profile from a few isolated pieces. Then, we compute the HTs of such points with respect to the family $\mathcal{F} = \{\mathcal{E}_{a,b,c,d}\}$ of ellipses, expressed in the cartesian form with four parameters:

$$\mathcal{E}_{a,b,c,d} : b^2(X - c)^2 + a^2(Y - d)^2 - a^2b^2 = 0,$$

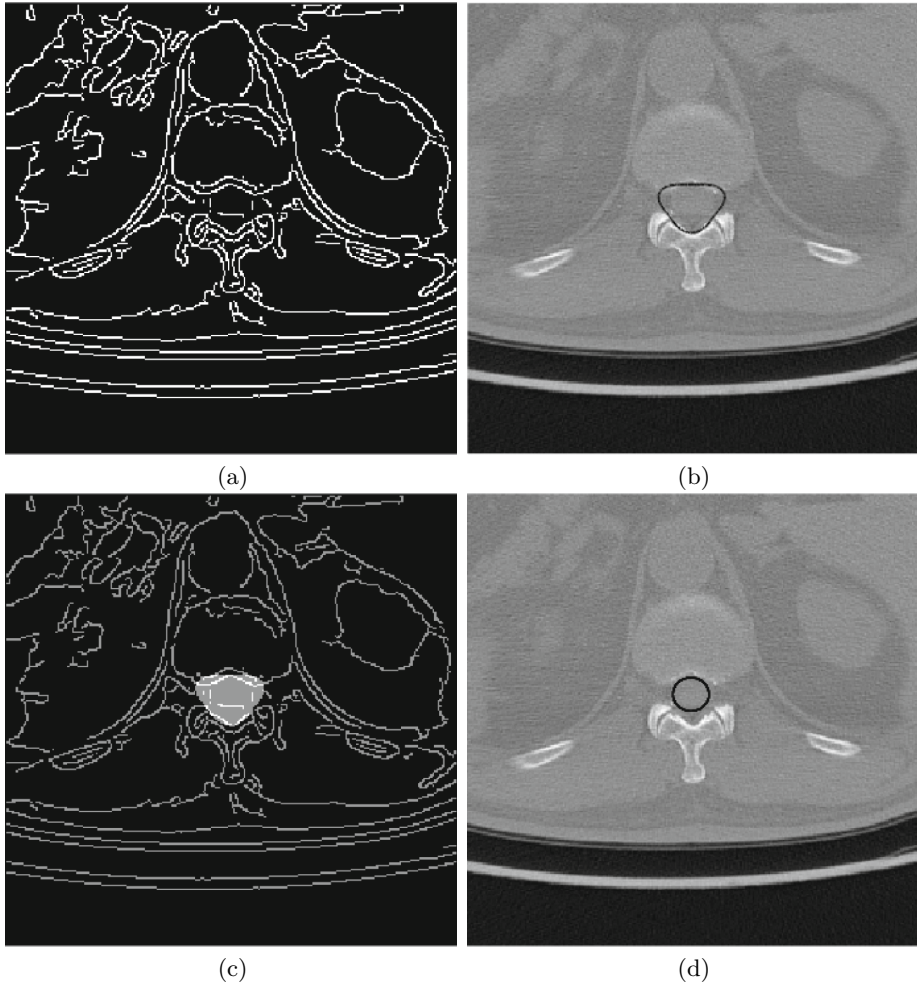


Fig. 3. First row: edge detection (a) and curve with 3 convexities (b) associated to the parameters ($a = 0.85$, $b = 0.15$) obtained by using the HT-based procedure. Second row: edge points (c) inside the region bounded by the curve with 3 convexities in (b) and the ellipse (d) detected by applying the HT-based procedure to the points highlighted in (c). The ellipse parameters are $a = 0.6$, $b = 0.65$, $c = -0.125$, $d = -0.025$.

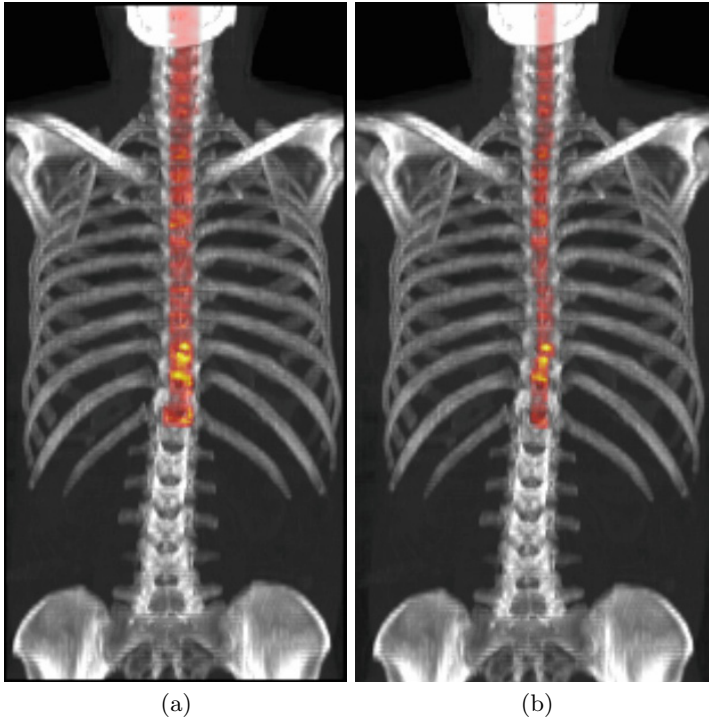


Fig. 4. PET activity of the whole spinal canal (a) and PET activity of the spinal marrow (b) for cervical and thoracic segments, superimposed to the original CT images in coronal view (color figure online).

where (c, d) is the center of the ellipse and the positive real numbers a, b play the role of semi-axes. The recognized curves (Figure 3: curve with 3 convexities in panel (b), and ellipse in panel (d)) are then used to create binary masks that can be applied to 180 PET images of the same subject, properly coregistered, each CT image corresponding to two PET images. Once the spinal canal and the spinal marrow are recognized and the corresponding binary masks are applied to the PET images, it is possible to quantitatively study the metabolic activity of the spinal district. In Figure 4 we show the activity of the whole spinal canal (panel (a)) together with the activity given just by the spinal marrow (panel (b)). Starting from the first PET image in the cervical segment and moving down to the last one in the thoracic segment, for each image we can compute the sum of the pixel values (i.e., the Standardized Uptake Value, SUV) in the spinal canal and in the spinal marrow. For the two Regions Of Interest (ROI) separately, we can compute the cumulative activity and the normalized cumulative activity

$$\text{SUV}_c(i) = \sum_{j=1}^i \text{SUV}(j), \quad i = 1, \dots, 180, \quad (8)$$

and the normalized cumulative activity

$$\text{SUV}_{\text{nc}}(i) = \frac{1}{i} \sum_{j=1}^i \text{SUV}(j), \quad i = 1, \dots, 180, \quad (9)$$

where $\text{SUV}(j)$ is the metabolic activity of the ROI in the j -th slice, and, of course, $\text{SUV}_c(180)$ ($\text{SUV}_{\text{nc}}(180)$) is the total activity (normalized total activity) along the vertebral column. Referring to the computation of (8) and (9), in Figure 5 we compare results obtained by using the HT-based procedure with the ones obtained by using the OsiriX software [11], whereby the ROIs are drawn manually by an expert user, slice by slice, and are used as ground truth. The overall behavior of the cumulative functions obtained via HT replicates the ground truth, with a good agreement in the case of the spinal canal activity evaluation. On the other hand, we can notice a slight underestimation of the spinal marrow activity. Finally, we point out that a comprehensive comparative analysis among the HT-based technique, when applied to the bone profile detection problem, and standard recognition/fitting techniques, such as the active contour model [12], the OsiriX package [11] and smoothing spline toolbox [13], is provided in [5, Section 5].

Remark 3. The use of two different recognition steps, the spinal canal first and then the spinal marrow, allows us to exclude the tissues out of the spinal district and to effectively analyze the activity within the canal. In particular, we are able to distinguish between the activity of the spinal marrow and the activity given by other tissues belonging to the spinal canal and surrounding the spinal marrow.

Remark 4. The benefit of using the curve with 3 convexities for recognizing the spinal canal is twofold. First, in [5, Section 5] it has been proved that curves from this family are able to adapt themselves to best approximate three different profiles of the spinal canal at different levels of the same vertebral column. This peculiar behavior makes the curve with 3 convexities a good candidate for the recognition of the spinal canal profiles across a whole stack of CT images. Second, the use of the curve with 3 convexities to limit the region where to search for the spinal marrow, gives us for free an upper bound for the semi-axes of the ellipse we use for the spinal marrow recognition. Accordingly, this allows us to optimize the parameter space discretization.

Remark 5. In medical imaging applications, the use of the HT-based technique leads to associate an equation to a specific bone or human tissue profile. However, the families of curves used in this paper display symmetries that are not perfectly preserved in humans. As a consequence, a more precise identification of tissue profiles would require a method to assign an appropriate piece of curve to a specific portion of the human district under investigation. To address this issue, a piecewise formulation of the HT technique is in progress (see [14]).

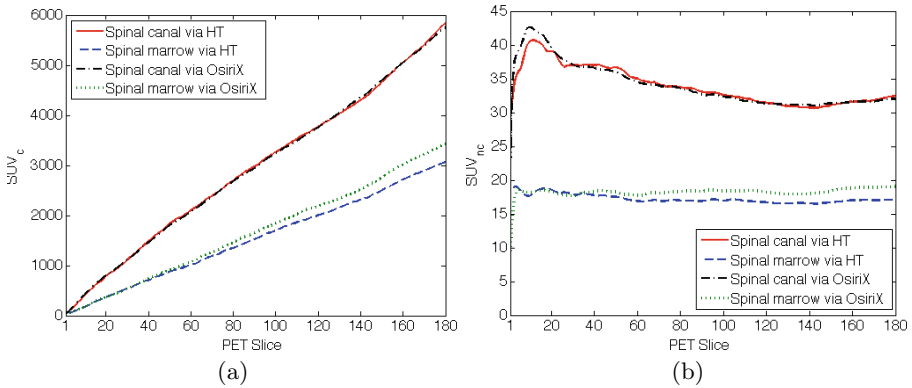


Fig. 5. The cumulative values of the SUV activity (a) and normalized SUV activity (b) across the PET slices for the spinal canal computed via HT (solid line) and via OsiriX (dash-dot line). The same quantities (again in panel (a) and (b), respectively) for the spinal marrow computed via HT (dashed line) and via OsiriX (dotted line).

4 Conclusions

In this paper we have presented a HT-based method for the segmentation of the spinal canal and spinal marrow in X-ray CT images. We have used different families of curves for the recognition of both the spinal canal and of the spinal marrow profiles, in order to separate the marrow from the surrounding tissue. Information inferred from the anatomical images has been integrated with functional information from PET images in order to quantitatively evaluate the metabolic activity of the spinal marrow with respect to the one of the whole canal. We have tested our method on a control subject, who does not present any neurological disease, before utilizing it in those cases where the knowledge of the activity of the spinal marrow is essential. In fact, its application to large datasets of neurological patients and control subjects could assess the presence of different levels of metabolic activity in the spinal canal and/or marrow and, thus, information on the nature of this kind of disease can be derived.

Acknowledgments. We wish to thank our colleague Michele Piana for many helpful discussions. We also thank Gianmario Sambuceti, Head of the Nuclear Medicine Unit of the IRCCS San Martino - IST, Genova, for providing us with the CT and PET images processed in this paper.

References

1. Hough, P.V.C.: Method and Means for Recognizing Complex Patterns. U.S. Patent 3069654 (1962)
2. Duda, R.O., Hart, P.E.: Use of the Hough transformation to detect lines and curves in pictures. *Commun. ACM* **15**(1), 11–15 (1972)

3. Ballard, D.H.: Generalizing the Hough transform to detect arbitrary shapes. *Pattern Recog.* **11**(2), 111–122 (1981)
4. Beltrametti, M.C., Massone, A.M., Piana, M.: Hough transform of special classes of curves. *SIAM J. Imaging Sci.* **6**, 391–312 (2013)
5. Massone, A.M., Perasso, A., Campi, C., Beltrametti, M.C.: Profile detection in medical and astronomical images by means of the Hough transform of special classes of curves. *J. Math. Imaging Vis.* **51**(2), 296–310 (2015)
6. Cistaro, A., et al.: Brain hypermetabolism in amyotrophic lateral sclerosis: a FDG PET study in ALS of spinal and bulbar onset. *Eur. J. Nucl. Med. Mol. Imaging* **39**, 251–259 (2012)
7. Hickman, S.J., et al.: Application of a B-spline Active Surface Technique to the Measurement of Cervical Cord Volume in Multiple Sclerosis From Three-Dimensional MR Images. *J. Magn. Reson. Imaging* **18**, 368–371 (2003)
8. Horsfield, M.A., et al.: Rapid semi-automated segmentation of the spinal cord from magnetic resonance images: Application in multiple sclerosis. *NeuroImage* **50**, 446–455 (2010)
9. Archip, N., et al.: A Knowledge-Based Approach to Automatic Detection of the Spinal Cord in CT Images. *IEEE Trans. Med. Imag.* **21**(12), 1504–1516 (2002)
10. Canny, J.F.: A computational approach to edge detection. *IEEE Trans. Pattern Anal. Mach. Intell. PAMI* **8**(6) 679–698 (1986)
11. Rosset, A., Spadola, L., Ratib, O.: OsiriX: an open-source software for navigating in multidimensional DICOM images. *J. Dig. Imag.* **17**(3), 205–216 (2004)
12. Aramini, R., Brignone, M., Coyle, J., Piana, M.: Postprocessing of the linear sampling method by means of deformable models. *SIAM J. Sci. Comput.* **30**(5), 2613–2634 (2008)
13. The MathWorks, Inc. <http://www.mathworks.com/help/curvefit/cftool.html> (accessed May 31, 2015)
14. Ricca, G., Beltrametti, M.C., Massone, A.M.: Piecewise recognition of bone skeleton profiles via an iterative Hough transform approach without re-voting. In: Ourselin, S., Styner, M.A. (eds.) *Proc. of SPIE Medical Imaging 2015: Image Processing*, vol. 9413, p. 94132M